Bubble Formation at Orifice in Viscoelastic Liquids

Koichi Terasaka and Hideki Tsuge
Dept. of Applied Chemistry, Keio University, Yokohama 223-0061, Japan

To evaluate the effect of viscoelasticity on bubble formation, four rheological parameters of viscoelastic liquids were defined and measured by a rheometer. The effects of operating conditions and concentration of polyacrylamide aqueous solutions (PAA) as viscoelastic liquids on bubble volume and the growth curve were experimentally measured. A high-speed video camera showed that the shapes of a bubble growing in viscoelastic liquids are not spherical. In this study, a nonspherical bubble formation model was proposed to theoretically estimate the volume, shape and growth curve of bubbles formed from an orifice submerged in viscoelastic liquids which are assumed to follow Maxwell's viscoelastic model. This experimental results in relatively low concentrations of PAA, as well as previous researchers' results, agreed relatively well with the calculated ones by this model.

Introduction

In the biochemical, food and polymer industries, some culture and polymer suspended media show non-Newtonian dynamic behavior such as pseudoplasticity and viscoelasticity. Because of the complex hydrodynamics of these fluids, it is difficult to estimate the mass transfer and mixing in these media. Especially in stirred tank bioreactors, the difference in shear stress between an impeller and wall in non-Newtonian liquids is larger than that in Newtonian liquids. Bubble columns show good mixing and more homogeneous shear stress profiles than stirred tanks so that these have been used for non-Newtonian media in polymerization reactors, bioreactors and/or fermentors. To design the bubble column type bio- and polymerization reactors for non-Newtonian fluids, it is essential to estimate the mass-transfer rate in the liquids. The mass-transfer rate depends on the gas-liquid contacting area so that the estimation of bubble size at a gas distributor is necessary in cases of relatively low gas-flow rate and/or low liquid height.

To design suitable gas distributors in bubble columns, Tsuge and Terasaka (1989) correlated the volume of bubbles formed from an orifice submerged in pseudoplastic non-Newtonian liquids and developed a dimensionless empirical equation whose accuracy is within $\pm 30\%$. To estimate the volume, shape and growth curve of a bubble and to clarify the bubble formation mechanism in pseudoplastic non-Newtonian liquids, Terasaka and Tsuge (1991) proposed a nonspherical bubble formation model for pseudoplastic fluids. Although the bubble volume, shape and growth curve in pseudoplastic liquids were well predicted by this model, the solutions during some fermentations and polymerizations show not only pseudoplastic rheological behavior but also viscoelasticity. There are few studies on bubble formation mechanisms and the volume of bubbles formed in viscoelastic liquids. Acharya et al. (1978) presented some experimental results in viscoelastic liquids as well as in pseudoplastic liquids, and a simple dimensional equation with a correlation factor so that bubble volume was estimated relatively well at high gas-flow rates. Räbiger and Vogelpohl (1986) obtained experimental results on the diameter of bubbles formed at an orifice submerged in polyacrylamide aqueous solutions (PAA) as viscoelastic liquids. Ghosh and Ulbrecht (1989) described the hydrodynamic characteristics of PAA aqueous solutions using the two-parameter version of Oldroyd's eight-constant model and proposed a nonspherical bubble formation model. The volumes of bubbles experimentally obtained at the detachment from an orifice under constant-flow conditions, where gas flows through the orifice at a constant flow rate, were compared with the calculated results.

In this study, the viscoelastic characteristics of the PAA aqueous solutions, which are typical polymer fluids, are approximated by the Maxwell model. Therefore, it is convenient and useful to estimate the effect of viscoelasticity on

Correspondence concerning this article should be addressed to K. Terasaka.

the bubble formation by this model. The volume, shape, and growth curve of a bubble formed at an orifice submerged in viscoelastic liquids were experimentally measured under the intermediate condition.

The bubble formation from an orifice is classified into three conditions. The first one is the *constant-flow condition*; the second one is the *constant pressure condition*, in which the pressure in the gas chamber established below the orifice is constant during bubble formation. Then, the third is the *intermediate condition* in which a bubble grows accompanied by pressure fluctuation in the gas chamber (Tsuge, 1986).

To evaluate the viscoelasticity of the liquids used, four dynamic viscoelasticity parameters were defined. By introducing these rheological parameters, the nonspherical bubble formation model was modified so that the bubble volume and growth curves computed by this model are compared with the experimental results as well as those by previous researchers.

Theoretical Studies

Estimations of elasticity and viscosity by rheometer

By using the coaxial double cylinder rheometer (MR-3 Soliquid Meter: Rheology Co.) which has a coaxial inner bob and outer cup, the dynamic elasticity G' (Pa) of liquid filled in the cup was measured as the ratio of differential shear stress acting on the bob $\dot{\tau}$ (Pa/s) to angular velocity of the oscillating cup ω (rad/s).

$$\dot{\tau} = G'\omega \tag{1}$$

The radial velocity profile of parallel liquid flow between cup and bob is expressed as $u = \omega y$, where y is the radial distance from the axis (m), so that the relation between the shear rate $\dot{\gamma}$ (s^{-1}) and angular velocity ω (rad/s) is

$$\dot{\gamma} = \frac{du}{dy} = \omega \tag{2}$$

Therefore, Eq. 1 is rewritten as follows

$$\dot{\tau} = G'\dot{\gamma} \tag{3}$$

In the PAA aqueous solutions as shown in Figure 1, the relation between log G' and log $\dot{\gamma}$ is linear as well as that between log μ and log $\dot{\gamma}$ so that elasticity G' is described by the power-law model as well as viscosity μ (Pa·s)

$$G' = p\dot{\gamma}^q \tag{4}$$

$$\mu = m\dot{\gamma}^{n-1} \tag{5}$$

where p, q, m, and n are the elasticity coefficient (Pa·s^q), elasticity index, viscous coefficient (Pa·s^n) and viscous index, respectively.

Thus, the relaxation time λ (s) is described as follows

$$\lambda = \frac{\mu}{G'} = \frac{m}{p}\dot{\gamma}^{n-q-1} \tag{6}$$

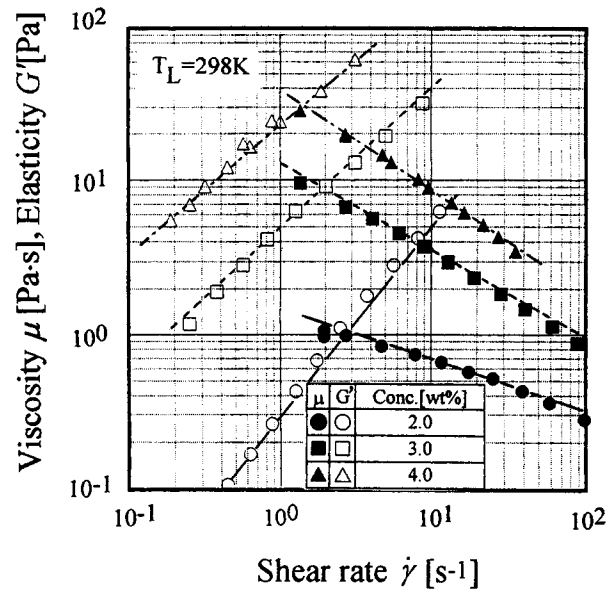

Figure 1. Rheological characteristics of PAA aqueous solutions.

Relation between shear stress and shear rate

The viscoelastic behavior of the PAA aqueous solutions were investigated using the creep and recovery tests, which measure the strain-response of solutions for a step-input of a constant value of shear stress, that is, 1.0 Pa for 8.6 s, by a rheometer (RheoStress RS500: HAAKE). To approximate the rheological characteristics of polymer solutions, there are two very simple viscoelastic models, that is, the Maxwell and Voigt models. Figure 2a shows the typical strain-response of Maxwell model fluids by the dotted line and Voigt model fluids by the chain line with an arbitrary vertical axis for a step input of constant shear stress by the solid line (Schramm, 1994). Since a strain of PAA solution increases instantaneously at $t = 0$ and a part of the strain is recovered at $t = 8.6$ for the step input of the shear stress during 8.6 s in Figures 2b–2d, those solutions behave as Maxwell fluids rather than Voigt ones.

Figures 2b–d show the strain responses of PAA aqueous solutions used in this study for the step input given in Figure 2a. As shown in Figures 2b–d, the viscoelastic characteristics of PAA aqueous solutions were approximately expressed by the Maxwell model; the response of 2.0 wt. % PAA aqueous solutions was in especially good agreement. Therefore, the rheological behavior of PAA solutions is assumed to be described as follows

$$\dot{\gamma} = \frac{\dot{\tau}}{G'} + \frac{\tau}{\mu} \tag{7}$$

where τ is the shear stress.

By solving Eq. 7 for τ

$$\tau = e^{-\int \frac{dt}{\lambda}}\left[\int e^{\int \frac{dt}{\lambda}} G'\dot{\gamma}dt + C\right] = e^{-\frac{t}{\lambda}}\left[\int e^{\frac{t}{\lambda}} G'\dot{\gamma}dt + C\right] \tag{8}$$

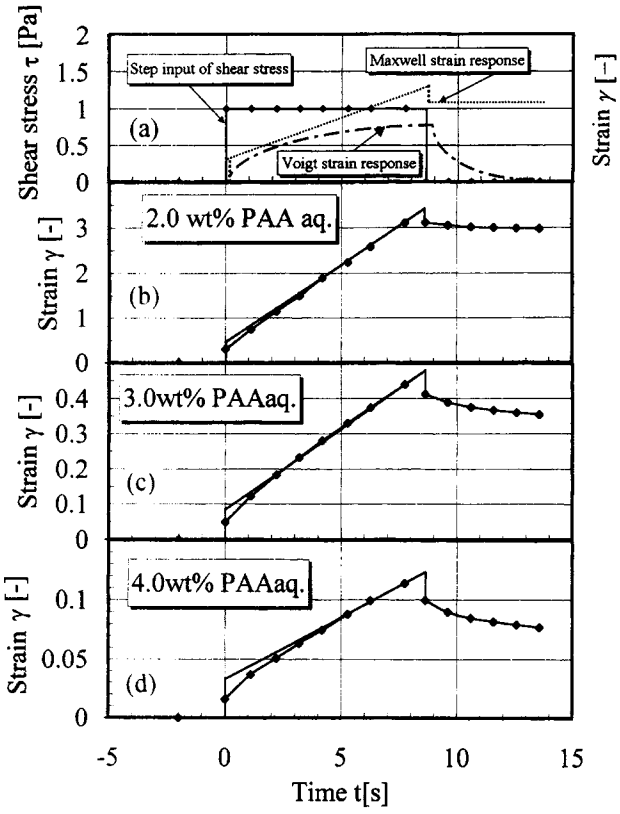

Figure 2. Creep and recovery tests of PAA solutions.

where the relaxation time $\lambda = \mu/G'$ and the constant $C = 0$ because of $\tau = 0$ and $\gamma = 0$ at $t = 0$.

Thus

$$\tau = e^{-\frac{t}{\lambda}}\left[\int e^{\frac{t}{\lambda}} G'\dot{\gamma}dt\right] \tag{9}$$

In the case of $\lambda \gg t$, the shear stress is described by the equation of elasticity as follows

$$\tau = \int G'\dot{\gamma}dt = G'\gamma \tag{10}$$

In the case of $\lambda \ll t$, the shear stress is described by the equation of viscosity as follows

$$\tau = \frac{e^{\frac{t}{\lambda}} G'\dot{\gamma}}{\frac{1}{\lambda}e^{\frac{t}{\lambda}}} = \mu\dot{\gamma} \tag{11}$$

Nonspherical bubble formation Model

To theoretically describe bubble formation at an orifice submerged in highly viscous Newtonian and pseudoplastic non-Newtonian liquids, Terasaka and Tsuge (1990, 1991) developed a nonspherical bubble formation model. In this study, that model is modified for application to bubble formation in viscoelastic liquids.

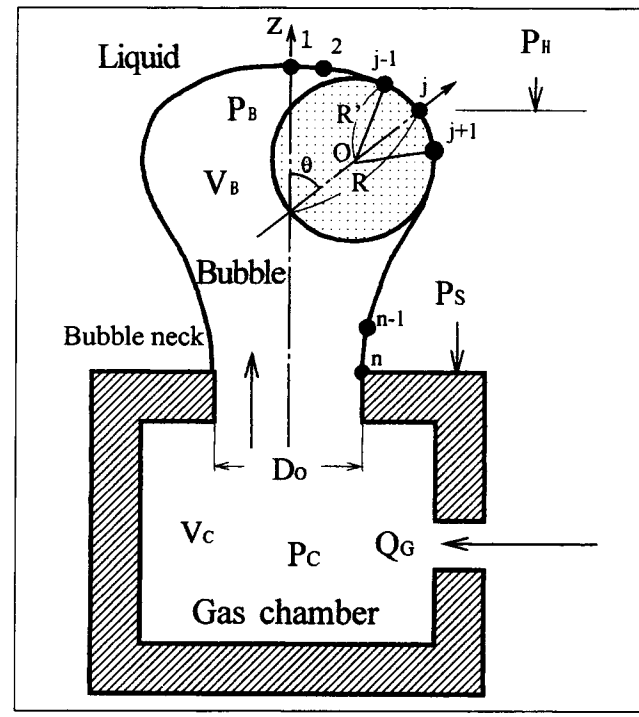

Figure 3. Nonspherical bubble formation model.

Concept of Nonspherical Model. In this model, the bubble surface is divided into a number of elements as shown in Figure 3. Gas flows into a gas chamber at the constant flow rate Q_G (m^3/s) so that pressure in the gas chamber P_C (Pa) increases. When the P_C becomes larger than the sum of the hydrodynamic pressure and surface tension, gas in the gas chamber begins to flow into the orifice and a bubble begins to expand.

Two motion equations in the radial and vertical directions are simultaneously solved so that the radial and vertical velocities for each element on the bubble surface are calculated and positions of those elements are estimated. This estimation is finished when the bubble detaches from an orifice, that is, the bubble neck is closed (Terasaka and Tsuge, 1990).

It is assumed that strain in a liquid does not exist at all before bubble growth, that is, $t < 0$. Namely, the bubble motion is not affected by the presence of other bubbles during bubble formation. Also, the bubble grows symmetrically about the vertical axis on the center of an orifice.

The equations describing these phenomena are formulated in the following manner.

Pressure Change in the Gas Chamber. As the behavior of gas in the gas chamber is assumed to be polytropic, the pressure change in the gas chamber is expressed as

$$\frac{dP_C}{dt} = \frac{\kappa P_C}{V_C}(Q_G - Q_O) = \frac{\kappa P_C}{V_C}\left(Q_G - \frac{dV_B}{dt}\right) \tag{12}$$

where Q_O and κ are the gas-flow rate through an orifice and polytropic coefficient, respectively. The value of κ (polytropic coefficient) is 1.1, which was experimentally obtained by Terasaka and Tsuge (1990).

Orifice Equation. The pressures in a bubble P_B (Pa) and in a gas chamber P_C (Pa) are assumed to be related by the orifice equation as follows

$$P_C - P_B = \frac{Q_O|Q_O|}{k_O^2} = \left(\frac{1}{k_O^2}\frac{dV_B}{dt}\right)\left|\frac{dV_B}{dt}\right| \tag{13}$$

The orifice constant k_O ($m^{7/2}/kg^{1/2}$) was experimentally determined by Terasaka and Tsuge (1990) as follows

$$k_O = 0.813 D_O^2 \tag{14}$$

where the units of k_O and D_O are $m^{7/2}/kg^{1/2}$ and m, respectively.

Definition of Equivalent Radii. The bubble surface is divided into a number of two-dimensional axisymmetric elements which are characterized by two principal radii of curvature R and R' (m), as shown in Figure 3. R' is the radius of the circle which passes through the elements $j-1$, j and $j+1$, and has a center point O. Another radius R is the distance from the bubble's symmetrical axis to the element j through point O and is defined as a characteristic radius at element j to calculate the inertial force of the bubble and shear stress of the bubble's surface.

On the other hand, $\bar{R}$ is defined by Eq. 15 to estimate the surface tension at element j

$$\frac{1}{\bar{R}} = \frac{1}{2}\left(\frac{1}{R} + \frac{1}{R'}\right) \tag{15}$$

Shear Rate at Bubble Surface. Scriven (1959) derived a motion equation of bubble expansion using the Navier-Poisson equation, where the radial shear rate from the bubble surface to infinity was analytically obtained as follows

$$\dot{\gamma} = \frac{4}{R}\frac{dR}{dt} \tag{16}$$

Pressure Balance on the Gas-Liquid Interface. On element j, it is postulated that the bubble shape is a sphere which has radius R. The expansion of the gas-liquid interface is defined by the following modified Rayleigh equation

$$P_B - P_H = \rho_L\left(|R|\frac{d^2R}{dt^2} + \frac{3}{2}\frac{dR}{dt}\left|\frac{dR}{dt}\right|\right) + \frac{2\sigma}{\bar{R}} + \tau \tag{17}$$

where P_H is the hydrostatic pressure at element j (Pa) and the three terms on the righthand side of Eq. 17 represent inertia, surface tension (N/m) and viscoelastic stress, respectively. The viscoelastic stress on the bubble surface τ is expressed by Eqs. 16 and 9

$$\tau = e^{-\frac{t}{\lambda}}\left[\int e^{\frac{t}{\lambda}} G'\left(\frac{4}{|R|}\frac{dR}{dt}\right)dt\right] \tag{18}$$

Motion Equation of a Rising Bubble. In the present model, the motion equation of a rising bubble is described by inertia, buoyance forces, surface tension at an orifice, gas momentum rate through an orifice, and viscoelastic forces

$$\frac{d}{dt}\left(M'\frac{dz}{dt}\right) = (\rho_L - \rho_G)V_B g - \pi D_O \sigma + \frac{4\rho_G|Q_O|Q_O}{\pi D_O^2} - \tau_z\frac{\pi D_M^2}{4} \tag{19}$$

where M' and D_M (m) are the virtual mass [$=(\rho_G + 11\rho_L/16)V_B g$)] and maximum horizontal bubble diameter. Vertical viscoelastic shear stress τ_z is defined as follows

$$\tau_z = e^{-\frac{t}{\lambda}}\left[\int e^{\frac{t}{\lambda}} G'\dot{\gamma}_z dt\right] \tag{20}$$

where $\dot{\gamma}_z$ (s^{-1}) is the vertical shear rate of a rising bubble described as follows

$$\dot{\gamma}_z = \frac{8}{D_M}\frac{dz}{dt} \tag{21}$$

Procedure to Solve the Model. The simultaneous differential equations described above are solved by the following procedures.

(1) Determining the initial gas chamber pressure by the orifice diameter and surface tension, that is $P_C = P_S + 4\sigma/D_O$.

(2) Estimating the gas chamber pressure by the mass balance equation in the gas chamber.

(3) Estimating the pressure in the bubble by solving the orifice equation.

(4) Calculating the equivalent radii R and $\bar{R}$ (m) at any element on the bubble surface.

(5) Evaluating the radial acceleration and velocity of the bubble surface by solving the pressure balance between the inside and outside of the bubble surface.

(6) Evaluating the vertical acceleration and velocity of the bubble by solving the motion equation of the rising bubble.

(7) This calculation finishes when the neck of the bubble is closed, that is, any element on the bubble surface except for the element on the top of bubble $j = 1$ contacts the symmetrical axis at the final condition.

Experimental Studies

Figure 4 shows the experimental apparatus. The bubble column has a 0.15 m square cross section and is 0.40 m high. N_2 gas flows uniformly into the gas chamber after measurement of the gas-flow rate. By assuming the bubble size is uniform, a single bubble volume was calculated by dividing the gas-flow rate by the frequency of bubble formation measured by the IR sensor (CU217: Keyence Co., Ltd.). The bubble shapes during bubble growth were recorded by a high speed video camera (EktaPro 1000: Kodak), and the bubble volumes were analyzed as a function of time with a video measuring gauge (IV-560: FOR-A Co., Ltd.) and personal computer (PC-9801VX: NEC).

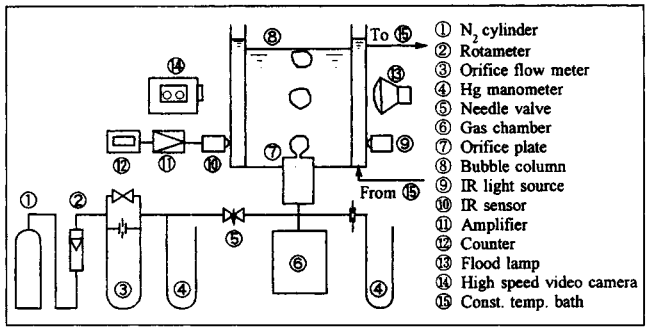

Figure 4. Experimental apparatus.

The operating conditions were as follows: gas-flow rate $Q_G = 0.2\times10^{-6}$–25×10^{-6} m^3/s, orifice diameter $D_O = 0.99\times10^{-3}$–2.04×10^{-3} m, gas chamber volume $V_C = 85.1\times10^{-6}$–415×10^{-6} m^3, and liquid height $H_L = 0.134$–0.150 m.

The liquids used were 2.0, 3.0 and 4.0 wt. % polyacrylamide (PAA) aqueous solutions (Aldrich Co., Ltd.) whose physical properties and rheological characteristics are described in Table 1. Their rheological parameters, surface tension, and density are experimentally measured by a co-axis double cylinders type rheometer (MR-3 Soliquid Meter: Rheology Co.), a CBVP-type surface tension meter (CBVP A-1: Kyowa Scientific Equipment Co.), and a hydrometer (Nippon Keiryoki Kogyo Co.), respectively.

Results and Discussion

Bubble growth curve

Figure 5 shows a comparison of the bubble growth curves between the experimental and calculated data by this model, which are presented by plots and lines, respectively. In the case of $Q_G = 0.542\times10^{-6}$ m^3/s under the condition in Figure 5, it was observed during bubble growth that the bubble volume temporarily decreases. It shows that gas-flow direction through an orifice change due to the pressure balance between the bubble and gas chamber. Especially, in the case of a small gas chamber volume, the pressure in the gas chamber sensitively changes during bubble growth. The time course of the bubble volume is well described by this model.

Relaxation time during bubble growth

Figure 6 shows the time course of the mean relaxation time $\bar{\lambda}$ during bubble growth under the same conditions as in Figure 5. The mean relaxation time $\bar{\lambda}$ which is averaged for all relaxation times of the elements on the bubble surface, was estimated by this model. In the cases of relatively high gas-flow rates ($Q_G = 5.36-10.7\times10^{-6}$ m^3/s), the relaxation time $\bar{\lambda}$ is smaller than the growth time t (s) except for the initial period of bubble growth so that the elasticity significantly affects the bubble growth for only the initial period of bubble formation. On the other hand, in the case of a low gas-flow rate ($Q_G = 0.542\times10^{-6}$ m^3/s), the elasticity influences the bubble growth at $t = 0.06$ s as well as the initial period because of the temporary decreasing bubble volume at that point.

Table 1. Physical and Rheological Properties of PAA Aqueous Solutions

Concentration (wt. %)	2.0	3.0	4.0
Viscosity coeff. m (Pa·s^n)	1.39	12.0	37.0
Viscosity index n	0.653	0.440	0.365
Elasticity coeff. p (Pa·s^q)	0.290	4.56	24.1
Elasticity index q	1.25	0.912	0.842
Liquid density ρ_L (kg/m^3)	1,005	1,007	1,010
Surface tension σ (N/m)	55.1×10^{-3}	65.1×10^{-3}	65.0×10^{-3}
Molecular weight		$\sim 5\times10^6$	

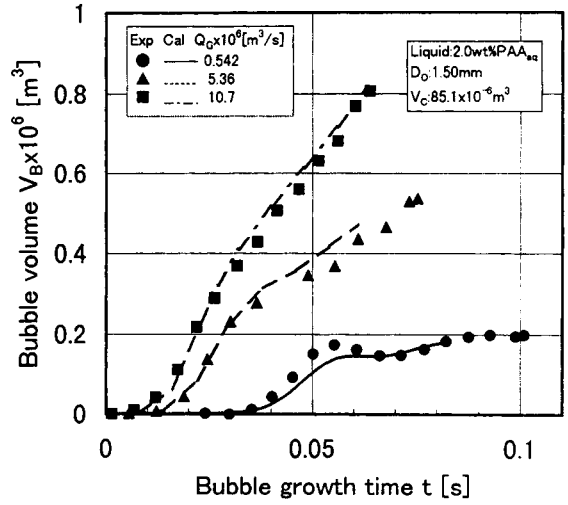

Figure 5. Bubble growth curves.

Bubble shape

Figure 7 shows the change in bubble shape during bubble growth at an orifice. The experimental bubble shapes were compared with the calculated ones using this model. For relatively low gas-flow rates, the experimental shapes were well estimated. At high gas-flow rates, however, a bubble was vertically stretched because of the large wake of the previous rising bubbles.

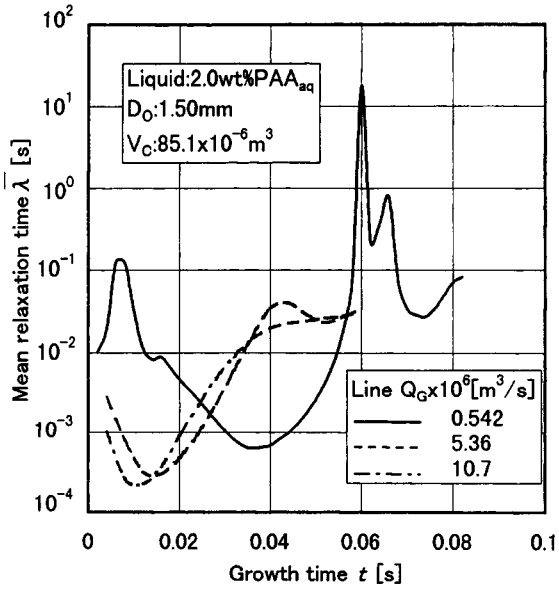

Figure 6. Mean relaxation time during bubble growth.

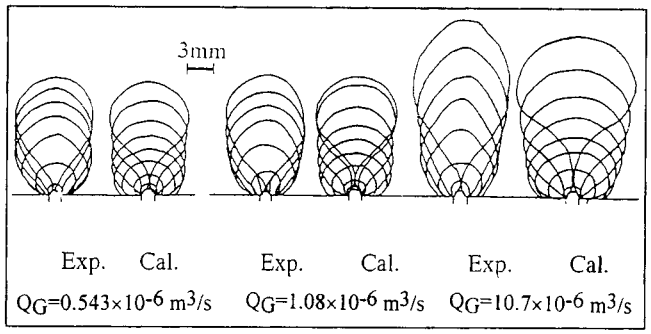

Figure 7. Bubble shapes: experimental vs. calculated results.

$D_O = 1.50$ mm; $V_C = 171 \times 10^{-6}$ m^3; 2.0 wt. % PAA_{aq}; Time interval: 10 ms.

Bubble volume

Effect of Gas Chamber Volume. Figure 8 shows the effect of the gas chamber volume V_C (m^3) on the relation between the bubble volume V_B (m^3) and the gas-flow rate Q_G (m^3/s). In the range of low gas-flow rate V_B increases with increasing V_C whereas, the difference in V_B is not observed any longer at $Q_G = 2 \times 10^{-5}$ m^3/s. This phenomenon is explained by the bubble formation mechanism. The gas fed into the gas chamber is accumulated up to $P_C \geqq P_S + 4\sigma/D_O$. For cases of low gas-flow rate and/or large gas chamber volume, a longer *waiting time*, which means the time period without bubble growth, is required so that the bubble volume depends on the chamber volume. On the other hand, for the case of high gas-flow rate, the waiting time is short enough so that the effect of the chamber volume on bubble volume is low. The calculated results using this model correspond well with experimental ones.

Effect of Orifice Diameter. Figure 9 shows the effect of orifice diameter D_O (m) on the relation between V_B and Q_G. Under the conditions in this figure, bubble volume decreases with increasing D_O in the range of $Q_G < 2 \times 10^{-6}$ m^3/s and increases with increasing D_O in the range of $Q_G > 2 \times 10^{-6}$ m^3/s. The pressure drop through an orifice increases with decreasing orifice diameter. In the case of low gas-flow rate, the smaller the orifice diameter, the longer the waiting time. On the other hand, for a high gas-flow rate, the smaller the orifice diameter, the more easily a bubble neck is closed. By using this model, that mechanism is well described as shown by the lines in Figure 8.

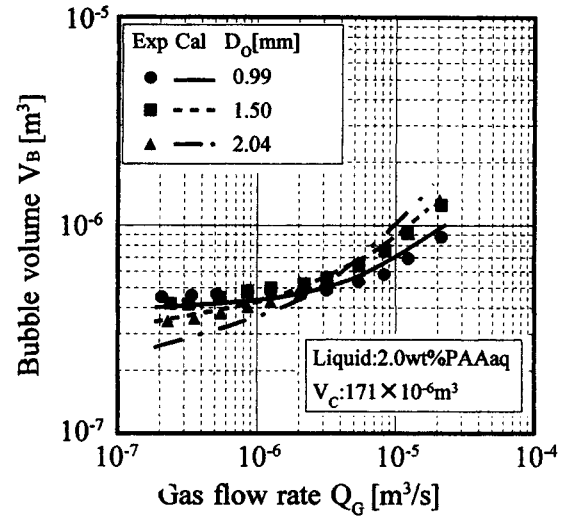

Figure 9. Effect of orifice diameter on relation between V_B and Q_G.

Effect of Concentration of PAA Aqueous Solutions. Figure 10 shows the effect of the PAA concentration on the relation between V_B and Q_G. The viscoelastic stress becomes larger with an increase in the concentration of PAA so that bubble growth time, which is defined as the time from the beginning of bubble formation to the detachment of the bubble, becomes longer and the volume of the detached bubble increases. For the cases of 2.0 and 3.0 wt. % PAA aqueous solutions, these experimental results are predicted relatively well by this model, whereas, the estimated bubble volumes

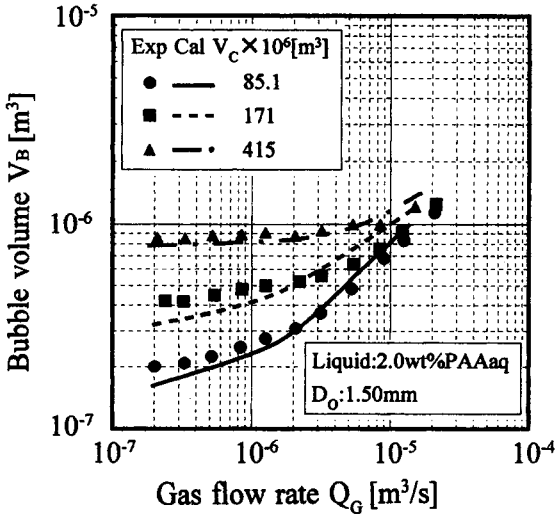

Figure 8. Effect of gas chamber volume on relation between V_B and Q_G.

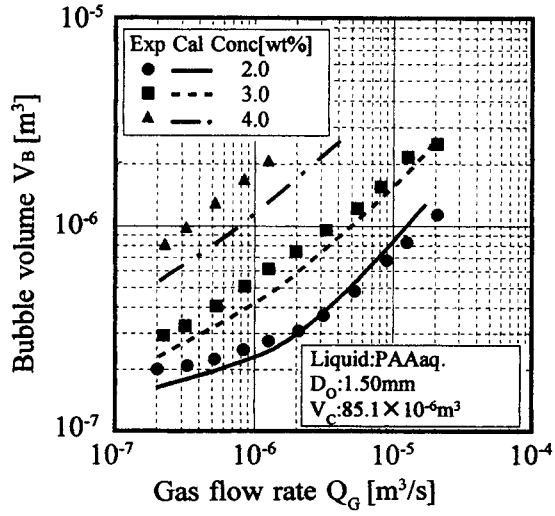

Figure 10. Effect of liquid concentration on relation between V_B and Q_G.

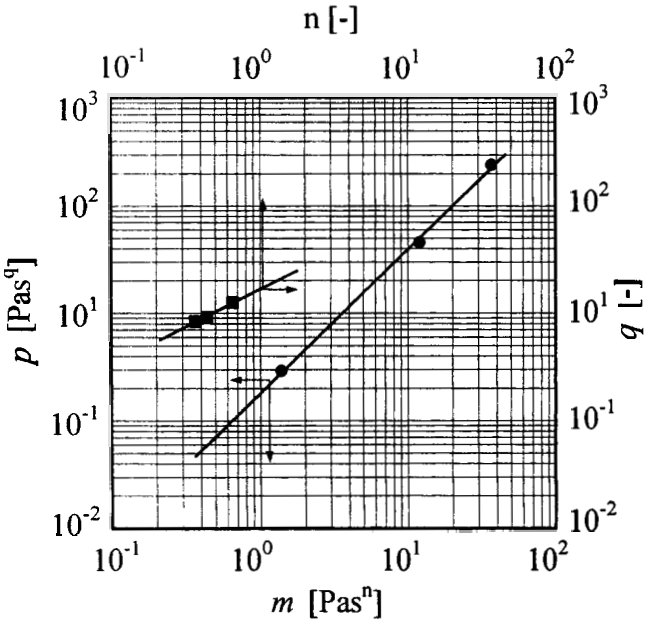

Figure 11. Correlations: p vs. m and q vs. n.

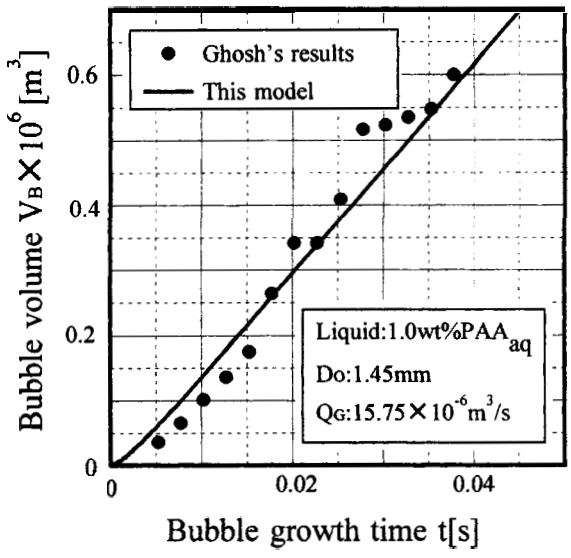

Figure 12. Ghosh's experimental growth and estimated model results.

are about 30% smaller than the experimental ones in the case of the 4.0 wt. % PAA solution. In the highly concentrated PAA liquids, their rheological behavior appears not able to be described well by the simple Maxwell model, as shown in Figure 2. For instance, for the case of 4.0 wt. % PAA solutions, the time course of strains is not completely proportional to time while the constant shear stress is acting on the liquids. This means that the concentrated PAA aqueous solutions have a more complicated rheological behavior.

Comparison with Previous Results

Räbiger and Vogelpohl (1986) and Ghosh and Ulbrecht (1989) obtained experimental results on bubble formation in PAA aqueous solutions. Their elasticity parameters such as p and q were unknown. To estimate these unknown values, the relations between the experimental results of p and m and between q and n were correlated in Figure 11. In the PAA aqueous solutions of this study, these relations are linear on the double-logarithmic plots, so that the unknown p and q values are evaluated by correlating the lines in Figure 10 with the other physical properties of PAA and their operating conditions as shown in Table 2.

The gas chambers used by Ghosh and Ulbrecht and Räbiger and Vogelpohl were small enough so that a *constant-flow condition* is assumed in these cases. Moreover, Räbiger and Vogelpohl (1986) operated at much higher gas-flow rates than that in this study.

Figure 12 shows the bubble growth curve evaluated by image analysis of the high speed simultaneous photographs in the article of Ghosh and Ulbrecht (1989) and the calculated results using this model. Under the experimental conditions of Ghosh and Ulbrecht, bubbles grow under constant-flow conditions. The calculated result shown by the solid line corresponds relatively well with the experimental one.

Figure 13 shows the bubble volumes estimated by this model and the model of Ghosh and Ulbrecht, as well as the experimental data from Ghosh and Ulbrecht (1989). Not only the model of Ghosh and Ulbrecht, but also this model estimated the bubble volume relatively well. At a high gas-flow rate, the calculated results using this model are slightly larger than the experimental ones because of the wake of the previous bubbles. On the other hand, at a low gas-flow rate where the effect of elasticity on bubble volume seems to be larger, the bubble volume calculated by this model corresponds well with the experimental data rather than that of Ghosh and Ulbrecht.

Table 2. Physical Properties and Operating Conditions of PAA Aqueous Solutions in Previous Studies

Researcher	Ghosh et al.			Räbiger et al.	
Orifice dia. D_O (mm)	1.45			2.0	
Gas flow rate Q_G (m^3/s)	**2.5×10^{-6}–17×10^{-6}**			0–83×10^{-6}	
Conc. (wt. %)	0.5	1.0	4.0	6.0	8.0
Liquid dens. ρ_L (kg/m^3)	**999.7**	**1002**	**1000***	1000*	1000*
Viscosity coeff. m (Pa·s^n)	0.08	0.60	0.16	0.19	0.52
Viscosity index n	0.770	0.700	0.62	0.61	0.52
Elasticity coeff. p (Pa·s^q)	0.0616*	0.0912*	0.0156*	0.0196*	0.0753*
Elasticity index q	1.38*	1.17*	1.19*	1.18*	1.06*
Surface tension σ (N/m)	70.66×10^{-3}	69.79×10^{-3}	65×10^{-3}	65×10^{-3}	65×10^{-3}

*Predicted values.

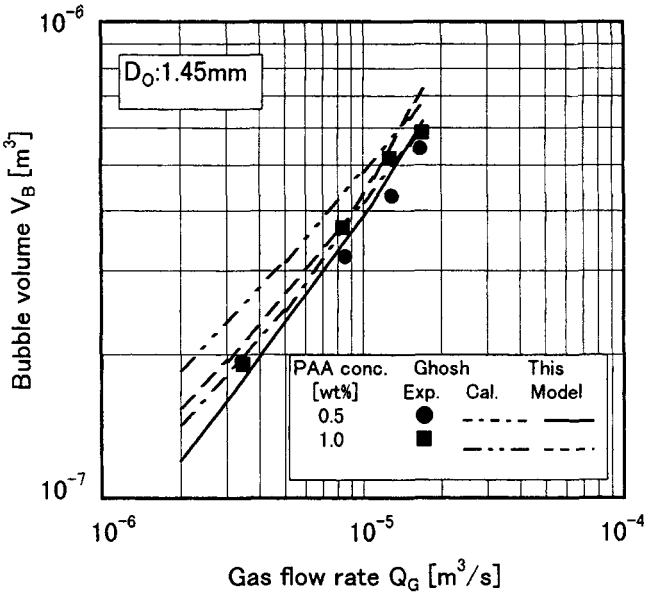

Figure 13. Ghosh's experimental and calculated bubble volumes and model results.

Although Ghosh and Ulbrecht (1989) have already proposed a bubble formation model for viscoelastic fluids using a two-parameter version of the Oldroyd model, it is more convenient to measure the dynamic elasticity and viscosity and use Maxwell's rheological model for many polymer solutions rather than Oldroyd's model.

Figure 14 shows a comparison between the experimental data of Räbiger and Vogelpohl (1986) and the calculated results of this model. Räbiger and Vogelpohl measured the bubble volume in the range of about 10–100-fold larger gas-flow rates than that in this experiment under constant-flow conditions, where the growing bubbles detach earlier from an orifice due to the wake of the previous rising bubbles because each bubble is not intermittently generated, but continuously,

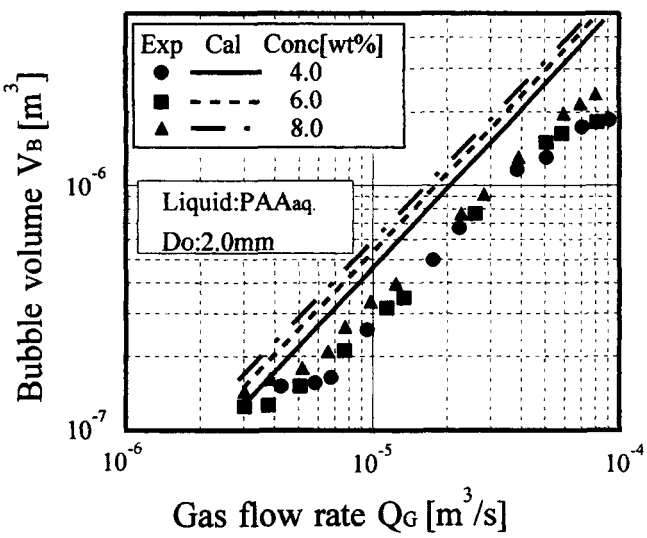

Figure 14. Räbiger's experimental data and calculated results of this model.

so that the distance between bubbles is very close and the hydrodynamic effect of a previously rising bubble is not neglected. Therefore, the calculated values are overestimated because of the assumption of no wake.

Conclusions

To estimate the shear stress acting on a gas-liquid interface of a growing bubble in viscoelastic liquids, four rheological parameters, p, q, m, and n, are measured using a coaxial cylindrical rheometer. The volume, shape, and growth curve of bubbles formed from an orifice submerged in 2.0 and 3.0 wt. % viscoelastic PAA aqueous solutions are well estimated by the nonspherical bubble formation model in which a viscoelastic fluid is described by the Maxwell model.

For the gas-flow rate where bubbles grow without the wake effect of the previous bubbles, previous researchers' experimental results as well as the present results were predicted relatively well by this model.

Acknowledgment

The authors are indebted to Mr. H. Hara for his assistance in this experiment.

Notation

g = gravitational acceleration, m/s^2
P_S = hydrostatic pressure at orifice plate, Pa
Q_O = gas-flow rate into bubble, m^3/s
T_L = temperature of liquid, K
u = radial liquid velocity in cup, m/s
z = vertical distance from orifice plate, m
γ = strain
θ = angle between the normal to bubble surface and vertical axis, rad
$\bar{\lambda}$ = mean relaxation time, s
ρ_G = gas density, kg/m^3

Literature Cited

Acharya, A., R. A. Mashelkar, and J. J. Ulbrecht, "Bubble Formation in Non-Newtonian Liquids," *Ind. Eng. Chem. Fundam.*, **17**(3), 230 (1978).

Ghosh, A. K., and J. J. Ulbrecht, "Bubble Formation from a Sparger in Polymer Solutions: I. Stagnant Liquid," *Chem. Eng. Sci.*, **44**, 957 (1989).

Räbiger, N., and A. Vogelpohl, "Bubble Formation and its Movement in Newtonian and Non-Newtonian Liquids," *Encyclopedia of Fluid Mechanics*, Gulf Publishing, Houston, p. 59 (1986).

Schramm, G., *A Practical Approach to Rheology and Rheometry*, Gebrueder HAAKE GmbH, Karlsruhe, Germany (1994).

Scriven, L. E., "On the Dynamics of Phase Growth," *Chem. Eng. Sci.*, **10**(1/2), 1 (1959).

Terasaka, K., and H. Tsuge, "Bubble Formation at a Single Orifice in Non-Newtonian Liquids," *Chem. Eng. Sci.*, **46**(1), 85 (1991).

Terasaka, K., and H. Tsuge, "Bubble Formation at a Single Orifice in Highly Viscous Liquids," *J. Chem. Eng. Japan*, **23**(2), 160 (1990).

Tsuge, H., "Hydrodynamics of Bubble Formation from Submerged Orifices," *Encyclopedia of Fluid Mechanics*, Vol. 3, Gulf Publishing, Houston, p. 191 (1986).

Tsuge, H., and K. Terasaka, "Volume of Bubbles Formed from an Orifice Submerged in Highly Viscous Newtonian and Non-Newtonian Liquids," *J. Chem. Eng. Japan*, **22**(4), 418 (1989).

Manuscript received Oct. 21, 1996, and revision received July 10, 1997.